Advances in Geo-Energy Research

Vol. 17, No. 1, p. 30-42, 2025

Original article

Experimental investigation into gas migration mechanism in submarine sandy sediments at pore-scale

Weilun Sun[1], Deqiong Kong[1,2], Zhenyi Li[1,2], Yu Peng[1], Yunmin Chen[1,2], Yi Pik Cheng[3], Bin Zhu[1,2]*

[1]*College of Civil Engineering and Architecture, Zhejiang University, Hangzhou 310058, P. R. China*

[2]*Center for Hypergravity Experimental and Interdisciplinary Research, Zhejiang University, Hangzhou 310058, P. R. China*

[3]*Department of Civil, Environmental and Geomatic Engineering, University College London, WC1E 6BT, United Kingdom*

Keywords:
Gas migration
marine geology
X-ray computed tomography
image analysis

Cited as:
Sun, W., Kong, D., Li, Z., Peng, Y., Chen, Y., Cheng, Y. P., Zhu, B. Experimental investigation into gas migration mechanism in submarine sandy sediments at pore-scale. Advances in Geo-Energy Research, 2025, 17(1): 30-42.
https://doi.org/10.46690/ager.2025.07.03

Abstract:
The dissociation of natural gas hydrate usually induces gas migration within shallow marine sediments, which has been widely reported to trigger geological hazards and submarine facility failure. To date, the mechanisms by which gas migration governs internal structural evolution and seafloor morphological changes remain poorly understood. This study investigates the gas migration behavior and associated morphological changes in sandy sediments using a novel experimental setup that integrates X-ray computed tomography scanning technology with a custom-built seepage apparatus. The apparatus enables gas injection with constant flow rate and real-time observation of the occurrence and migration process of gas within sediments. Experiments were conducted on Fujian sand with different particle sizes and gas flow rates, demonstrating that gas migration follows a particle-displacement pattern in fine-grained sediments and a pore-invasion pattern otherwise. The study further explores the dynamics of gas pocket formation, as well as the channel healing and re-opening behavior. The results demonstrate the pore-scale mechanism governing morphological evolution of seabed, with pockmarks and knolls at the surface and elongated chimney-like channels underneath. This work also highlights the advantage of X-ray computed tomography techniques for understanding gas migration processes in marine sediments.

1. Introduction

Gases are prevalent within marine sediments on a global scale, playing a critical role in shaping seabed morphology and influencing the chemical composition of seawater and the atmosphere. Therefore, the processes governing their occurrence and migration have attracted significant attention across various scientific disciplines. Submarine gases commonly appear as layered accumulations, columnar plumes, high-pressure gas pockets (i.e., gas-filled cavities), or gas hydrates. Regarding their composition, methane dominates, accompanied by minor amounts of carbon dioxide, nitrogen and other trace gases (Claypool and Kaplan, 1974; Claypool and Kvenvolden, 1983; Xu et al., 2017).

In complex marine environments, gases can escape from their sources through the sealing layers of the sedimentary seabed, forming pathways such as fractures. This process often leads to geological hazards and certain phenomena, as shown in Fig. 1, including pockmarks (i.e., circular or oval depressions), gas chimneys, and submarine landslides, which provide insights into deep-earth fluid dynamics and are key indicators of petroleum and natural gas resources (Clarke and Cleverly, 1991; Orange et al., 2008; Pape et al., 2014; Ma et al., 2021). Research demonstrates that such submarine gas systems hold strategic significance in the global energy landscape, with their vast untapped reserves presenting

Yandy Scientific Press

*Corresponding author.
E-mail address: weilunsun@zju.edu.cn (W. Sun); deqiong_kong@zju.edu.cn (D. Kong); Lizhenyi_1997@zju.edu.cn (Z. Li); zjupengyu@zju.edu.cn (Y. Peng); chenyunmin@zju.edu.cn (Y. Chen); yi.cheng@ucl.ac.uk (Y. P. Cheng).

Received May 4, 2025; revised June 5, 2025; accepted June 27, 2025; available online July 3, 2025.

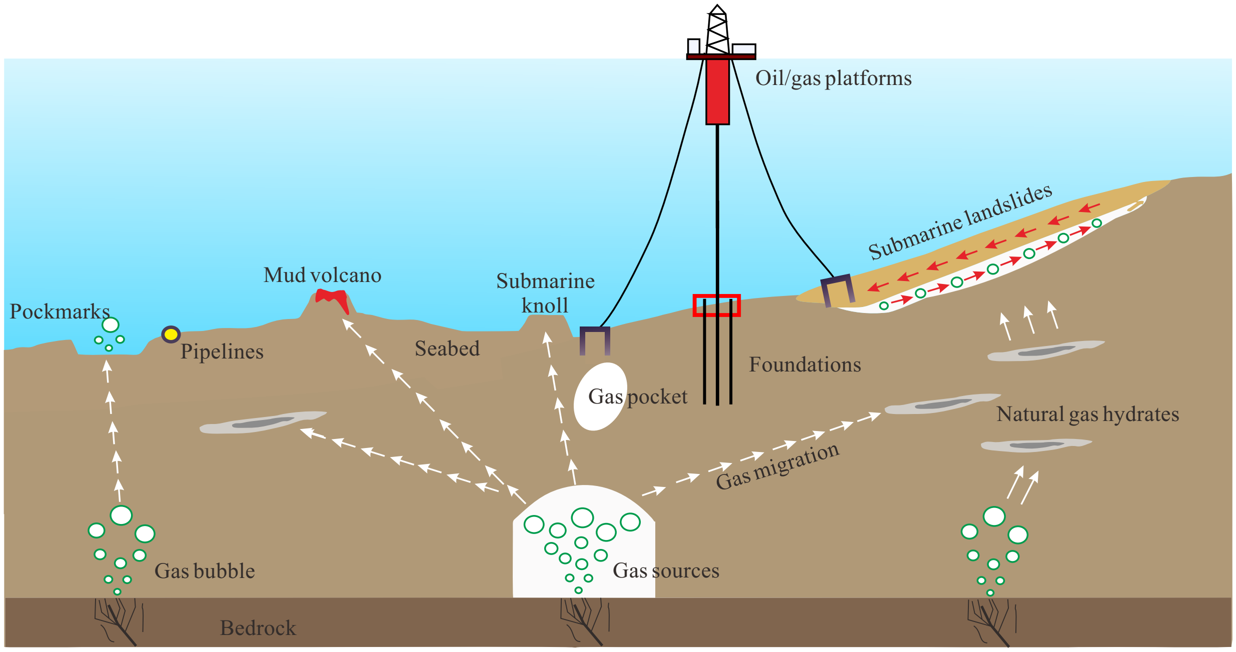

Fig. 1. Special geological structures and catastrophic geology induced by submarine gas migration.

extraordinary extraction prospects that could reshape energy geopolitics. Notably, the carbon equivalent stored in marine gas hydrates, estimated at between 500 and 10,000 Gt (Cao et al., 2025), may reach several times that of all proven fossil fuel reserves combined. This immense energy potential positions marine gas hydrates as a focal point for future energy development.

However, the release and migration of these gases can also significantly impact seabed stability (Puzrin et al., 2011; Sultan et al., 2012) by altering sediment pore structure, increasing pore pressure and reducing effective stress. In turn, such changes affect seabed properties like permeability, strength and stiffness, posing risks to offshore infrastructures, including platforms and pipelines (Fig. 1). For instance, a blowout in the Gulf of Mexico occurred during drilling operations failing to account for a high-pressure gas reservoir beneath the seabed (Rogener et al., 2018). Similarly, during the 2001 geological surveys for the Cross-Sea Bridge in Hangzhou Bay, China, drilling into shallow gas deposits triggered a blowout and seabed liquefaction. This incident resulted in fires on multiple offshore vessels and severe economic losses (Yan, 2020). Therefore, a systematic investigation of gas migration behaviors in marine sediments is critical to analyze the evolutionary patterns of associated geological phenomena and develop early-warning systems to mitigate risks to marine extraction infrastructure.

Recent technological advancements have significantly enhanced *in-situ* detection and sampling capacities for marine sediment studies. Notably, Sultan et al. (2020) conducted a four-day *in-situ* monitoring campaign at the West Svalbard margin, measuring pore pressure and temperature within the methane penetration zone to quantify gas flow dynamics in porous media. Yoneda et al. (2019) evaluated sediment permeability using intact cores from the Krishna-Godavari Basin. For large-scale characterization, acoustic techniques (e.g., high-resolution seafloor seismic profiling) have proven effective in mapping topographical features linked to subsurface geological processes (Cartwright and Santamarina, 2015; Wei et al., 2020). Furthermore, remotely operated vehicles enable direct visual documentation of seafloor manifestations of gas migration (Flohr et al., 2021).

Building upon *in-situ* observations, investigation into the gas migration mechanism in marine sediments and porous media have advanced through multidisciplinary approaches. Numerical simulations, such as discrete element and finite element modeling, have been used to replicate gas invasion processes and associated sediment responses (Jain and Juanes, 2009; Sirhan et al., 2019). More recently, Wang et al. (2025b) employed a Coupled Eulerian-Lagrangian method to investigate gas migration behavior in low-permeability marine sediment, for the first time capturing the entire gas invasion and rising process and accounting for the large deformation effect and soil strength softening. Furthermore, advancements in experimental visualization techniques, employing transparent soil analogs, microfluidic devices, and other innovative methodologies, have provided critical pore-scale insights (Choi et al., 2011; Liu et al., 2016; Campbell et al., 2017; Sun and Santamarina, 2019). These collective efforts reveal distinct migration patterns: In sandy sediments, gases predominantly accumulate along bedding planes or undergo rapid ebullition into the water column, whereas clay-rich sediments facilitate vertical gas migration through fracture networks.

In clay sediments, submarine gases often migrate in ellipsoidal (Barry et al., 2010) or teardrop-shaped (Algar et al., 2011) morphologies, a process well-described by Linear Elastic Fracture Mechanics (Johnson et al., 2002; Jain and Juanes, 2009; Barry et al., 2010; Roche et al., 2021). Migration begins when the difference between gas pressure p_g and the minimum principal stress σ_H exceeds the cohesion σ_C, causing initial fractures. This pressure difference cannot be dissipated immediately, leading to the development of linear fractures and interconnected channel networks.

In contrast, gas migration through sandy sediments, characterized by larger particle and pore sizes, exhibit more complex transport mechanisms. These are governed by capillary forces, viscous forces, and effective stress (Holtzman et al., 2012). Surface tension between seawater and the invading gas generates "capillary" cohesion, causing gas migration to exhibit a behavior that resembles fracture propagation in clay sediments or manifests unique capillary invasion patterns specific to sandy sediments.

However, the understanding of the gas pocket morphological evolution during migration through sandy sediments and the subsequent formation of geological features remains limited due to the following: (1) Scarce long-term *in-situ* observations, and (2) the inherent limitations of numerical and analytical modelling approaches. Existing visualization techniques, primarily employing plate models or microfluidic devices, provide valuable insights, and these methods are fundamentally restricted to Two-Dimensional (2D) or quasi-2.5-dimensional approximations of the migration process. Furthermore, the use of material substitutes (e.g., transparent soil analogs) in such experiments introduces additional constraints on accurately replicating Three-Dimensional (3D) gas migration dynamics and associated seabed morphological transformations in natural sediment systems.

This study investigates pore-scale mechanisms governing gas migration-induced morphological changes in sandy sediments, encompassing both internal structural evolution and seafloor deformation. Recent advancements in X-Ray Computed Tomography (CT) have revolutionized 3D characterization of sediment mechanical behaviors and phase transition dynamics (Kong and Fonseca, 2018; Lei et al., 2019; Seol et al., 2019; Cai et al., 2020; Guo et al., 2024). Leveraging these developments, we introduce a new CT-seepage apparatus that synergistically combines unit-cell scale experimental control with microscopic dimensional analysis during constant gas flow conditions. Our integrated approach enables the exploration of gas migration effects, including:

1) The genesis of characteristic seafloor features (e.g., knolls and pockmarks) through surface topography alteration;
2) Quantitative 3D characterization of gas pocket morphology (spatial distribution, size evolution);
3) Geomechanically sediment-gas interaction mechanisms.

2. Materials and methods

It is widely recognized that capillary action plays a pivotal role in determining gas migration patterns in sandy sediments. The capillary entry pressure P_C has long been described using expressions derived from the Young-Laplace equation. This pressure is directly proportional to the surface tension γ between seawater and the invading gas and inversely proportional to the pore throat radius r_{th}. This relationship can be expressed as follows (Mason and Morrow, 1991; Patzek, 2001):

$$P_C = \frac{2\gamma}{r_{th}} F(\theta, G, D) \tag{1}$$

where F denotes a function of the contact angle between the gas-water interface and the solid surface θ, the throat shape factor G and the throat corner angles D. As for the behavior of gas invasion into sediments, $F(\theta, G, D) \approx 1$ (Lenormand et al., 1983; Jain and Juanes, 2009), indicating little effect of the shape factors. The surface tension between water and the invading gas primarily composed of methane can be negligibly affected by changes (Biscay et al., 2009) in the absence of thermal effects, and r_{th} is related to the sediment grain size d. Thus, at a certain depth beneath the sandy seabed, the pressure difference between invading gas and water p_g-p_w (or the gas flow rate v_g) and d collectively determine the gas migration behavior.

2.1 Experimental apparatus design

The experimental system is powered by a custom-built battery, enabling fully independent operation of the sediment sample, gas source, water source, and flow control pump within the CT scanner, as illustrated in Fig. 2(a). By eliminating the need for external power supplies and shortening the length of flow pipelines, this design enhances both operational flexibility and control precision. Unlike conventional gas flow controllers that often struggle to maintain stable, low-speed and constant gas injection rate, this device uses a piston container made of 304 stainless steel (material with high strength and excellent sealing properties) to store gas. Gas is injected into the sediment via water displacement, ensuring a highly precise delivery rate of 0.01 mL/min, as verified through an extensive set of tests conducted in our lab.

The CT-compatible apparatus developed by Iglauer et al. (2011) and Lin et al. (2019) achieved exceptional gas injection capabilities for low-permeability rock cores, with operational pressures typically in the MPa range to overcome the low permeability of sandstone formations. In contrast, our design prioritizes the distinct requirements of very loose sandy sediments, employing: (1) A precision pressure control system (0-200 kPa range at a precision of 0.01 kPa), and (2) a Plexiglass (Polymethyl Methacrylate, PMMA) core holder optimized for granular material containment. The core holder has an inner diameter of 50 mm and a maximum allowable height of 50 mm (Fig. 2(b)). The gas injection needle, with an outer diameter of 1.5 mm and an inner diameter of 1.3 mm, minimizes boundary effects on gas migration within the core holder. Fluid pressures at the inlet and outlet are monitored by Sensor 1 and 2, respectively, at a data recording rate of 50-70 times per second. A porous polyether ether ketone board facilitates efficient drainage of fluids from the sample chamber, while flexible tubing is used for all pipelines to accommodate the rotation of the core holder during CT scanning. However, the current apparatus exhibits limitations in simultaneously achieving precise MPa-range pressure control and cryogenic condition regulation. These technical constraints are to be addressed in our forthcoming investigations focusing on the influence of natural gas hydrate phase transition dynamics on gas migration patterns.

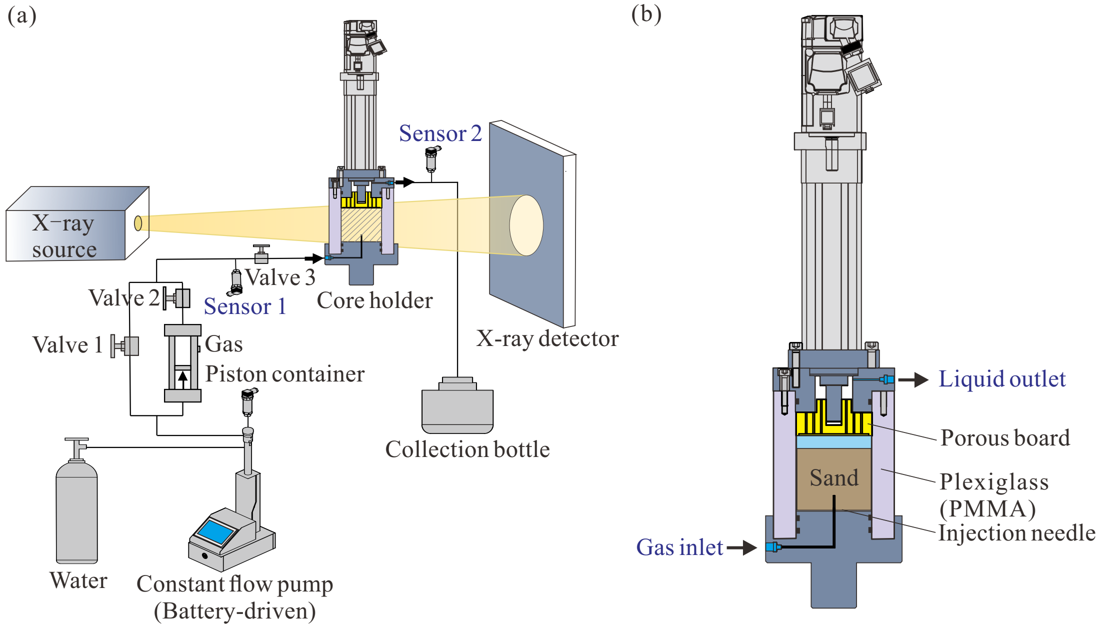

Fig. 2. Sketch of test apparatus: (a) Experimental system and (b) structure of the core holder.

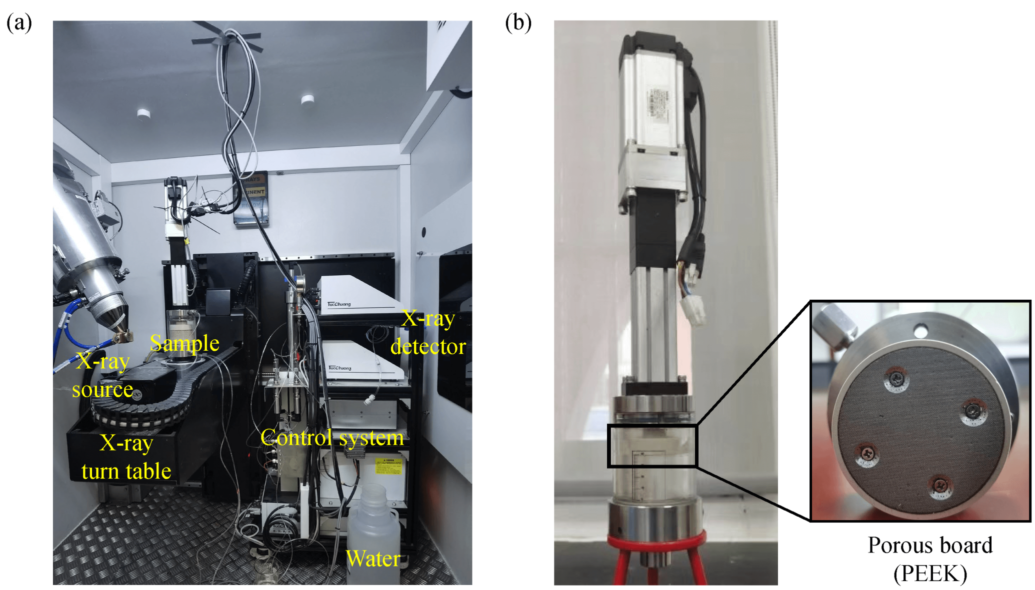

Fig. 3. Experimental device: (a) Configuration of the micro-ct scanner and (b) core holder and porous board.

2.2 CT parameters

The experiment was conducted at Zhejiang University using a Nikon XTH 225/320 LC CT scanner. The core holder was deliberately mounted on the rotating platform positioned between the X-ray source and the detector (Fig. 3).

Tomographic reconstruction was performed using the Nikon CT scanner's integrated software "CT Pro3D". On the basis of preliminary tests, the optimal scanning parameters were determined to be 145 kV and 110 μA, providing a resolution of 33.41 μm per voxel. This resolution enables precise characterization of gas bubbles larger than 1.0×10^{-3} mm^3, while also allowing for clear differentiation between distinct phases within the sediment sample. The complete 3D scan required approximately 40 minutes, acquiring ∼2,500 projections with a 1,000 ms exposure time per projection. Preprocessing (beam hardening correction, noise reduction, and data reconstruction) was performed using CT Pro 3D, yielding raw 3D data files. Subsequent postprocessing in Avizo included multiphase segmentation (based on watershed algorithm) and 3D rendering, following established micro-CT protocols for porous media (Lu, 2024).

2.3 Materials

The material to prepare the sediment sample used in the experiments was Fujian sand, from Pingtan Island off the east coast of China, characterized by an average particle size of 0.7 mm, particle size ranging from 0.075 to 1.40 mm, and a specific gravity of solid particles of 2.68. Deionized water, p-

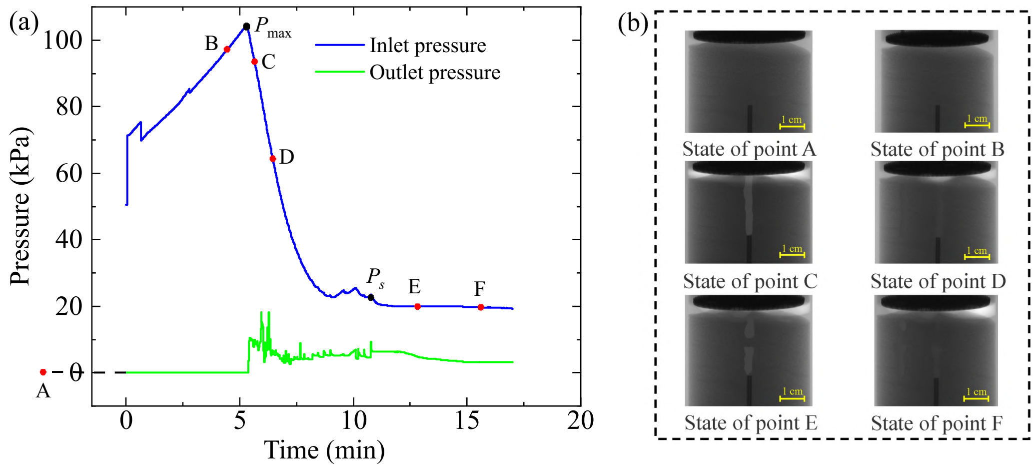

Fig. 4. Results of the gas injection experiment: (a) The gas pressure curve and (b) 2D X-ray projections at points A-F.

Table 1. Summary of test conditions.

No.	Particle size (mm)	Flow rate (mL/min)
CG	0.15-0.30	10
DS-1	0.30-0.60	10
DS-2	0.60-1.18	10
DS-3	1.18-1.40	10
DS-4	0.075-1.40	10
DR-1	0.15-0.30	1
DR-2	0.15-0.30	20

Notes: CG is control group, DS is different particle size and DR is different flow rate.

re-treated through vacuuming to remove dissolved gases, was used in the experiments to ensure consistency and to minimize interference from extraneous variables. Nitrogen gas was chosen as the gas source because of its non-polar molecular nature as well as molecular weight and viscosity closely resembling those of methane. No pre-equilibration of gas and water was required prior to gas injection because the gas dissolution effects are negligible in our experimental system, as confirmed by two key factors: (1) The deliberate selection of nitrogen gas to replicate methane's characteristic insolubility in natural marine sediments, and (2) the extremely low dissolution rate of gas bubbles in water.

2.4 Test procedure and conditions

All experimental procedures were conducted within the CT scanner. After sieving the sand samples into specific particle size ranges, the relative density of each sample group was controlled at 60% using the sand rain method. To minimize damage to the PMMA caused by the upper flange, Vaseline was applied to the top inner wall of the core holder. Water was then injected through a needle at a rate of 0.10 mL/min until the outflow volume reached 1.5 times the sample volume, ensuring full saturation of the sediment. The initial state of the sediment prior to gas injection was recorded by CT scanning.

Nitrogen gas, pressurized to a specified initial value, was stored in a piston container. The inlet valve was then opened to inject nitrogen gas into the sediment, and the full time trace of pressure throughout the process was recorded. Once the pressure-time curve stabilized, CT scanning commenced, with 2D X-ray projections being continuously captured to document the state of gas migration. The key parameters investigated were the particle sizes and flow rates, and the details of tests (empirically grouped based on sedimentological characteristics, e.g., Gong and Wang (2022) and Wang et al. (2025a)) are summarized in Table 1.

3. Results

3.1 Typical gas migration process

Fig. 4(a) presents the typical time trace of gas pressure throughout the gas migration process, with sample of particle size ranging from 0.15 to 0.3 mm and a constant injection rate of 10 mL/min. The experimental results reveal that the gas migration process in sandy sediments progresses through three distinct stages: Pressure accumulation, gas release, and channel healing.

3.1.1 Pressure accumulation

The inlet gas pressure curve as monitored by Sensor 1 (see Fig. 4(a)) initially exhibits moderate fluctuations and then increases linearly to a peak value ($P_{\max}$) at 318 seconds. During this period, gas bubbles begin to emerge from the needle tip, but the gas pressure is insufficient to overcome the combined resistance of effective stress, pore water stress, surface tension at the injection needle, and the capillary barrier formed by the porous board. As a result, no effective gas flow channel is formed. This absence of gas flow channel formation is further confirmed by the non-detectable outlet pressure, as measured by Sensor 2 (Fig. 4(a)), as well as the stable structure from Point A to Point B presented in Fig. 4(b).

3.1.2 Gas release

In the second stage, the gas pressure decreases from $P_{\max}$ to a lower value (P_S) at 651 seconds. Once the gas pressure

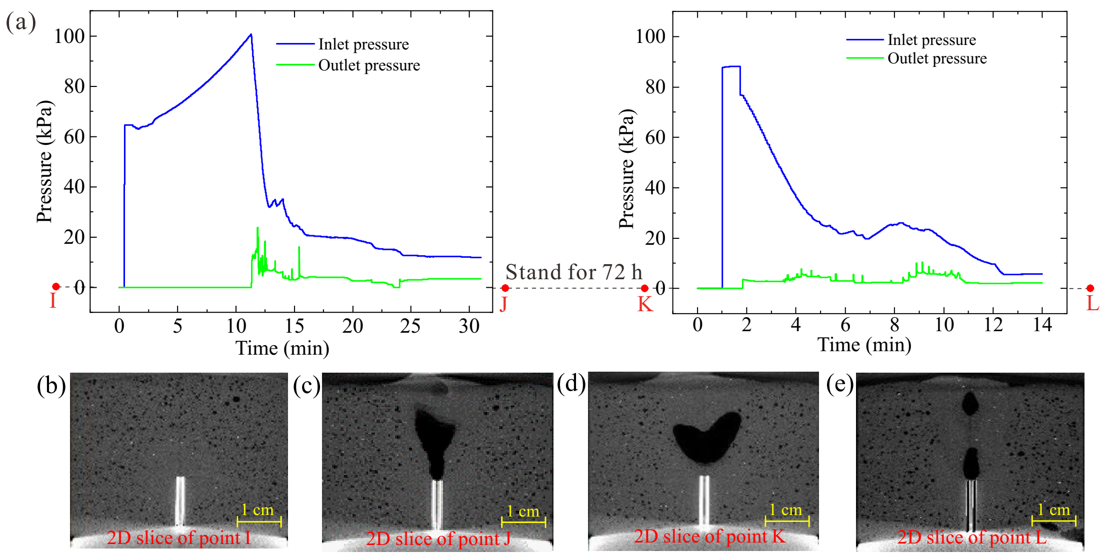

Fig. 5. Results of the complete gas migration experiment combined with CT 3D reconstruction: (a) Gas pressure curve and (b)-(e) the 2D slices of points I, J, K, L respectively represent the sediment states before and after the first gas migration and those before and after the secondary gas migration.

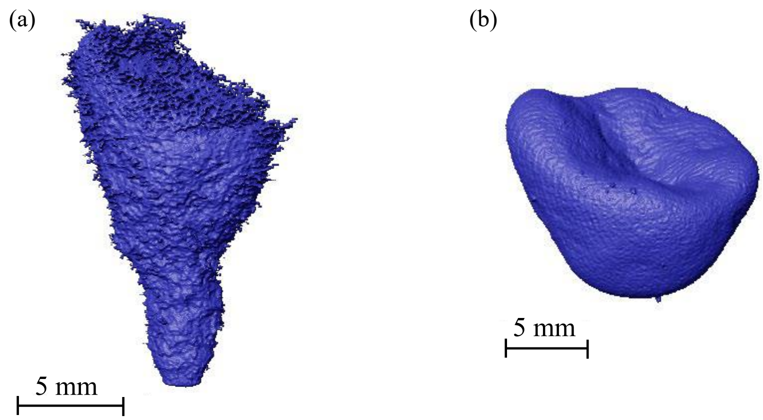

Fig. 6. 3D structure of gas morphology: (a) Morphological characteristics at point J and (b) morphological characteristics at point K.

surpasses the combined resistance, it rapidly penetrates the sediment, causing gas breakthrough and forming a continuous gas flow channel, as indicated by points C and D in Fig. 4(b). During this stage, the inlet pressure shows a significant drop, while the outlet pressure appears but then decreases slightly.

3.1.3 Channel healing

In the third stage, the gas pressure remains around the same level, stabilizes near P_S and slightly decreases over time. During this stage, the pressure is no longer sufficient to maintain the gas channel, resulting in sediment backfilling and subsequent healing of the open channel, as observed at the states of points E and F in Fig. 4(b).

To explore the further evolutionary behavior of gas, another set of sediment samples, which had previously undergone gas breakthrough, was left stationary on the CT tray for 72 h. Following this period, gas injection was repeated under the same conditions as the initial injection to simulate a secondary gas eruption into the sediment (Fig. 5). The pressure curve from the second injection reveals no distinct breakthrough point compared to the first, indicating that the initial gas intrusion has caused significant damage to the sediment structure, which cannot fully recover in such a period. During secondary gas migration, the migration path follows a similar trajectory to the initial invasion but releases more gas into the surrounding water. This leads to a reduction in the size of the original gas pocket, unless the lower part of the sediment remains continuously filled with a gas source.

Figs. 6(a) and 6(b) present the 3D reconstruction images corresponding to the states of points J and K in Fig. 5, respectively, visually illustrating the changes in the shape of gas pockets within the sediment during the dormancy period (i.e., when gas intrusion ceases). At point J, the gas pocket is of an irregular conical structure with a total volume of approximately 829 mm^3, denoting major and minor axis lengths of 17.82 and 8.65 mm, respectively. At point K, the

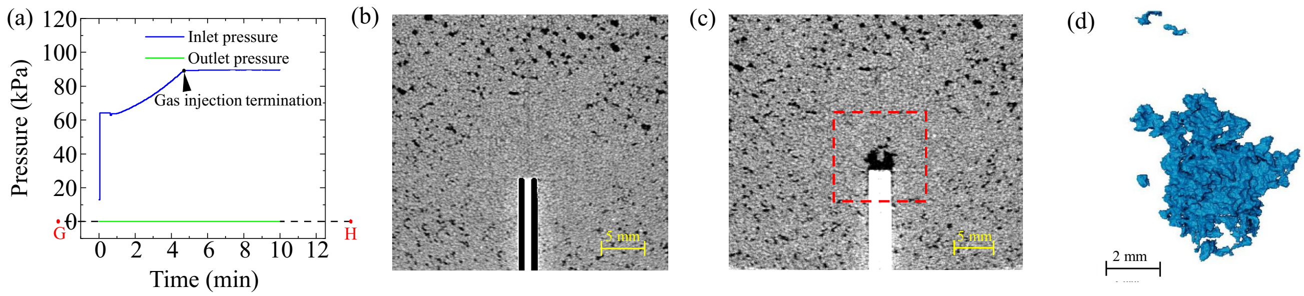

Fig. 7. Independent experiment for verifying internal conditions during gas accumulation period: (a) Gas pressure curve, (b) 2D slice of the state of point G, (c) 2D slice of the state of point H and (d) 3D structure of the red dotted box in (c).

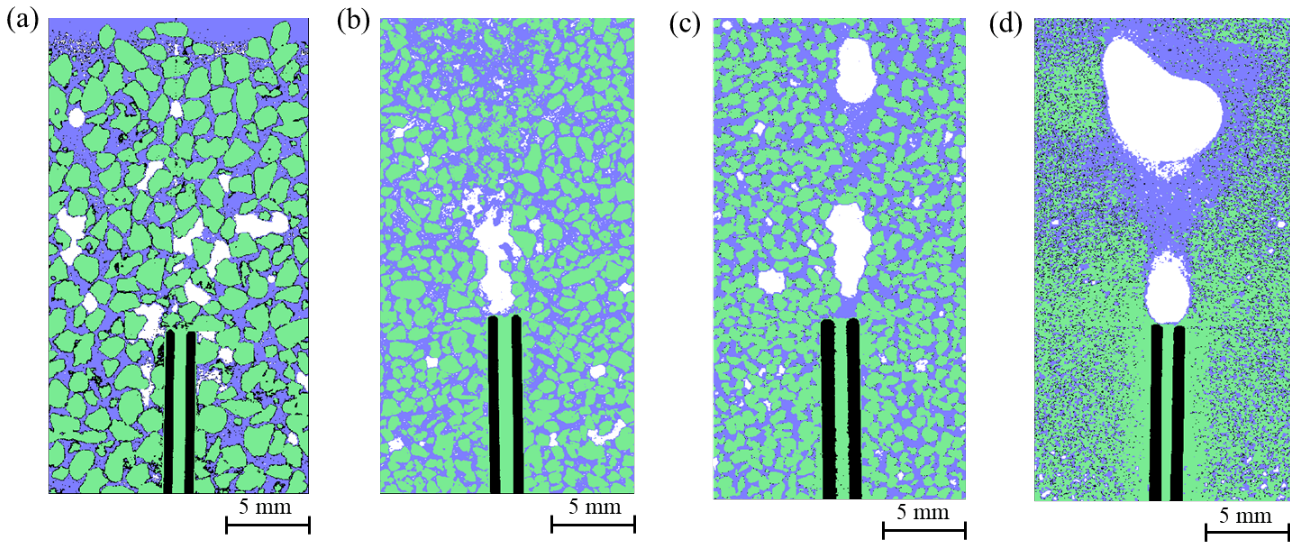

Fig. 8. Gas migration patterns at different particle sizes: (a) $d = 1.18$-1.40 mm, (b) $d = 0.60$-1.18 mm, (c) $d = 0.30$-0.60 mm and (d) $d = 0.15$-0.30 mm. Gas, water and sand particles are marked in white, blue and green, respectively.

gas pocket exhibits a constricted heart shape with a moderately expanded volume of 916 mm^3. The major axis length reduces to 15.65 mm while the minor axis length increases to 9.2 mm.

An independent validation experiment for the pressure accumulation stage, using sand samples with an identical particle size range (0.15-0.3 mm) to those in Fig. 4, was performed as illustrated in Fig. 7. Gas injection was terminated upon exceeding 80 kPa (Fig. 7(a)) to maintain first-stage migration behavior. The results confirmed the absence of channel formation, with only an irregular near-spherical bubble observed at the injection needle tip (Figs. 7(c) and 7(d)).

It should be noted that minor residual gas bubbles ((visible as black dots in Figs. 5(b) and 7(b)) were present in samples prior to gas injection due to the inherent characteristics of the sand-raining preparation method. Although small amounts of residual gas might exist in the initial sample, these isolated bubbles did not significantly influence the key gas migration pathways as observed in our replicative experiments.

3.2 Effect of particle size

The following four sets of experiments investigated the effect of particle sizes on the gas migration behavior. The corresponding 2D CT slices are shown in Fig. 8.

In sediments with a particle size range of 1.18 to 1.40 mm, disturbance is minimal, and there is little evidence of the formation of gas pockets. This can be partly attributed to the fact that a larger pore size, r_{th}, results in a lower capillary entry pressure, P_C, allowing gas to preferentially escape into the water through capillary action. In sediments with a particle size range of 0.60 to 1.18 mm, no significant changes are observed in the upper section but small gas pockets develop above the injection point. Hence, the increase in P_C leads to gas-induced fracture, thereby opening flow channels. For sediments with particle sizes between 0.30 and 0.60 mm, gas pockets form throughout the entire depth of the sediment, indicating the formation of continuous flow channels due to sediment fracturing. In sediments with the largest particle sizes between 0.15 and 0.30 mm, substantial disturbance occurs, resulting in the formation of large, irregular conical cavities.

Overall, large gas pockets do not form in sandy sediments with large particle sizes. As the particle size d decreases, the capillary entry pressure P_C increases, which changes the gas migration mode. Consequently, the gas is more likely to become trapped within the sediment, forming gas pockets rather than being released into the surrounding water.

Figs. 9(a) and 9(b) respectively show the surface profile and

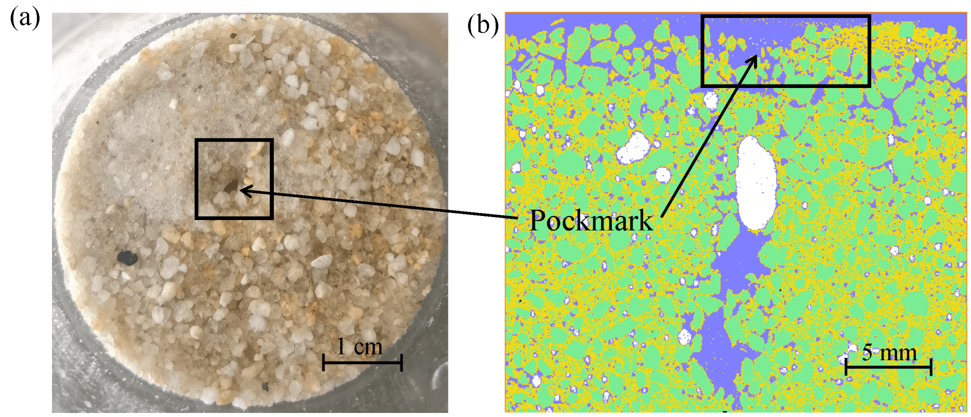

Fig. 9. Gas injection experiment result for the particle size range of 0.075 to 1.40 mm: (a) A photo of sediment surface and (b) the internal CT image. White stands for gas, blue for water, green for sand, and yellow represents a mixture of fine sand and water. The black boxes in (a) and (b) represent pockmarks formed after gas injection.

internal CT scans of the sand (particle size ranging from 0.075 to 1.40 mm) after gas injection. Due to the resolution limits of our CT imaging system, the segmentation between fine sand and water within this specific grayscale range cannot be further refined. However, this technical limitation does not affect our core findings, as the gas phase distribution–the primary focus of our analysis-remains clearly distinguishable and fully quantifiable across all experimental conditions. Inside the sediment, just above the gas injection point, an elongated fracture is visible. A distinct "pockmark" formed on the sand surface, encircled by a pronounced accumulation of finer particles that have been transported upward from deeper sediment layers by the gas migration process. This resulted in a significantly smaller average particle size within the "pockmark" compared to the surrounding sediments, a phenomenon consistent with Pau et al. (2014)'s observation at a pockmark site in the southwest Barents Sea.

3.3 Effect of gas injection rates

It has been noticed that the geomorphological features of the seabed exhibit strong correlation with gas invasion states, e.g., flow rate. This is further explored in Fig. 10. At a high flow rate (as shown in the case of $v = 20$ mL/min in Fig. 10), a large number of fine particles are entrained by the strong gas flow to the sediment surface; in field conditions, these particles could potentially be carried away by bottom currents, resulting in the formation of prominent pockmarks on the seabed surface. Thus, the sediment interior is left with an elongated, chimney-like gas channel. When the flow rate is reduced (as shown in the case of $v = 10$ mL/min in Fig. 10), the gas fails to entrain enough sediment, causing the seabed surface to be uplifted and resulting in the formation of knolls. At even lower flow rates (as shown in the case of $v = 1$ mL/min in Fig. 10), no significant changes occur on the seabed surface, which in the field may appear as a series of small-scale pits or elevations.

The morphology of gas pockets is closely linked to the surface features of the sediment, as shown in Fig. 10. Regardless of the gas rates, the gas migration always progresses in the normal direction toward the concave surface of the sediment (illustrated by the yellow arrows). In other words, the gas migrates and breaks through along the weakest areas of the sediment layers. When the gas supply is sufficient, it continues to propagate and develop along the channels, eventually reaching the seabed surface.

4. Analysis and discussion

Our CT-based experiments provide real-time, high-resolution visualization of gas occurrence and migration dynamics within sediments. Based on the findings in Section 3, this section examines: (1) The pore-scale mechanism linking gas migration to geological hazards, and (2) the multi-stage gas migration behavior. It is worth noting that the pressure accumulation stage is excluded from this analysis, as it induces negligible damage or morphological changes in sandy systems. Subsequent stages will be analyzed through the lens of particle-scale dynamics.

4.1 Entrainment effect

The occurrence of seafloor geological hazards is closely linked to localized uplift or subsidence, driven by gas invasion into sediments or the release of seafloor gas into the water column. This process arises from the displacement and loss of sediment particles during gas-liquid migration.

When gas entrains sand particles, the pore fluid exerts three dominant forces: Buoyancy, gas-driven force, and viscous drag. These forces collectively govern particle motion that shows strong dependence on the gas flow rate v_g. When v_g exceeds the natural settling rate of sediment particles, the gas flow dislodges particles from their original positions (Yan et al., 2021). This displacement disrupts inter-particle forces, initiating a chain reaction of particle movement that progressively weakens the sediment structure and facilitates the development of distinctive geological features.

In the experiments detailed in Section 3.2, flow rate was controlled at 10 mL/min, corresponding to a rate of 12.56 cm/s. At this rate, particles with diameters smaller than 1.14 mm are readily entrained by gas flow (see the "Particle entr-

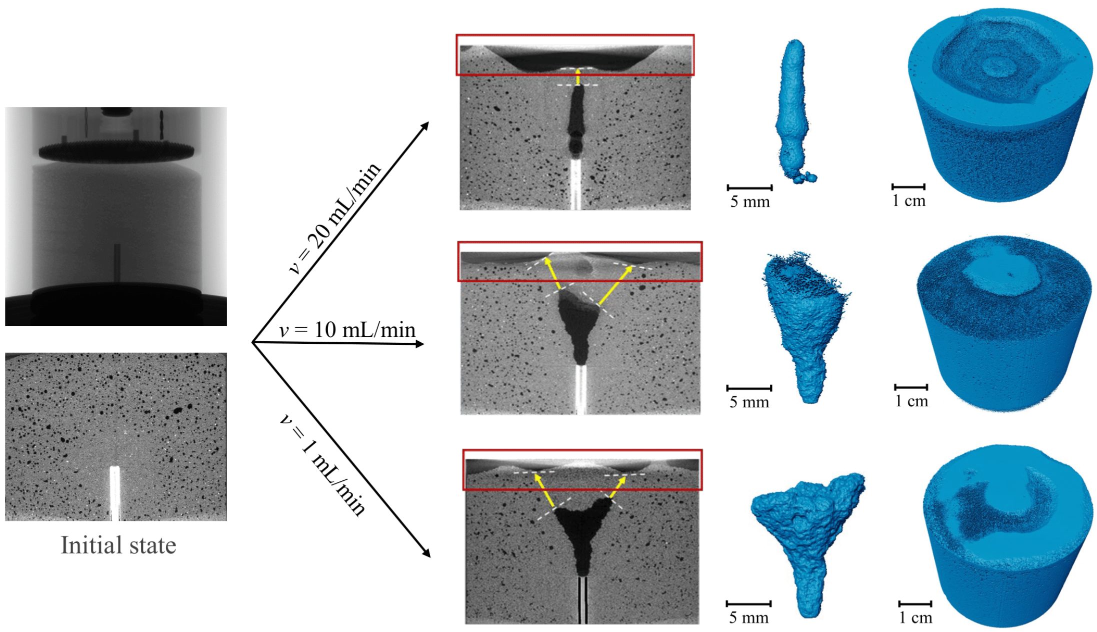

Fig. 10. Typical geological structures generated at different flow rates: $v = 1$, 10 and 20 mL/min.

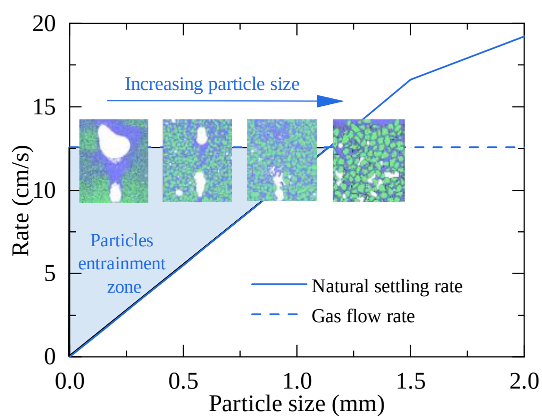

Fig. 11. Visual illustration of "Entrainment Effect". The natural settling rate is given by improved Goncharov formulas (Yan et al., 2021) and the gas flow rate is the experimental gas injection rate. The four CT images are consistent with Fig. 8.

ainment zone" in Fig. 11), while for particles greater than this value, their displacement becomes negligible due to the pore-invasion mechanism. Fig. 11 further demonstrates that the more pronounced "Entrainment Effect" exhibited by finer particles leads to intensified sediment structure disruption and the formation of a large gas pocket. This finding underscores the susceptibility of finer-grained sediments to geological hazards, as they are more prone to displacement and structural destabilization under gas flow conditions.

4.2 Channel healing

As demonstrated in Section 3, sediment channels undergo "self-healing" when either the gas supply ceases or the gas pressure becomes insufficient. Fig. 12 documents the morphological evolution of gas pockets over ∼1 hour after injection cessation, including 20 minutes of particle settling and 40 minutes of CT scanning. During this period, sand particles progressively infiltrate and occupy the gas pockets. This phenomenon is observed not only in sandy sediments but also in clay sediments, as previously noted by Sun and Santamarina (2019). However, the underlying mechanisms driving this behavior remain inadequately understood, and no conclusive hypothesis has been proposed.

The observed phenomenon may be interpreted as quasi-static flows, wherein the weak fluctuations around the gas pocket induce particle movement. These weak disturbances generate a localized "fluidization" effect (Kou et al., 2017), in which drag forces scale linearly with particle transport rates. This interaction between gas and sediment particles leads to the slow collapse and re-arrangement of the sediment structure around the gas pocket. The governing equation for particle motion around the gas pocket is given by (Srivastava et al., 2021):

$$m_s \dot{v}_s = \Delta\rho g V_S + F_r(t) - k\eta L v_s \tag{2}$$

where m_s and v_s respectively represent the mass and transport rate of the sediment particles, while g represents the gravitational acceleration of Earth. The first term on the right represents the buoyant force acting on the particles with volume V_S in the multiphase system due to the density difference $\Delta\rho$, the second term $F_r(t)$ refers to a random force exerted on the particles by the gas pocket, and the third term is the drag exerted on the particles during transportation, where k denotes the linear proportionality coefficient, η denotes the apparent viscosity and L is the characteristic length.

In quasi-static flows problems, the particle inertia can be reasonably neglected and the above equation can be further expressed as:

$$v_s = \frac{\Delta\rho g V_S + F_r(t)}{k\eta L} \tag{3}$$

Srivastava et al. (2021) expressed $F_r(t)/k\eta L$ as the function

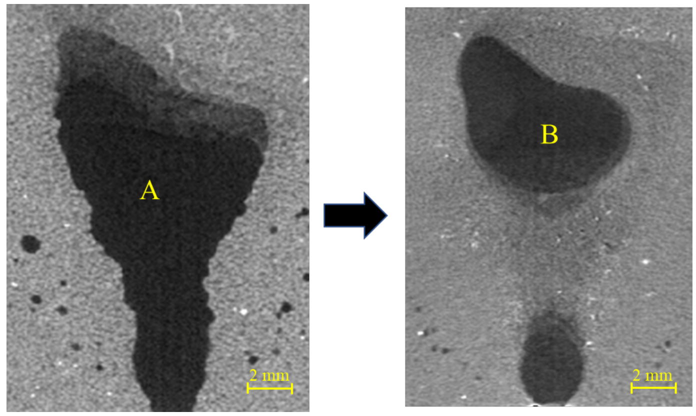

Fig. 12. Visualization of healing mechanism through X-ray image (From A to B). The black areas represent gas.

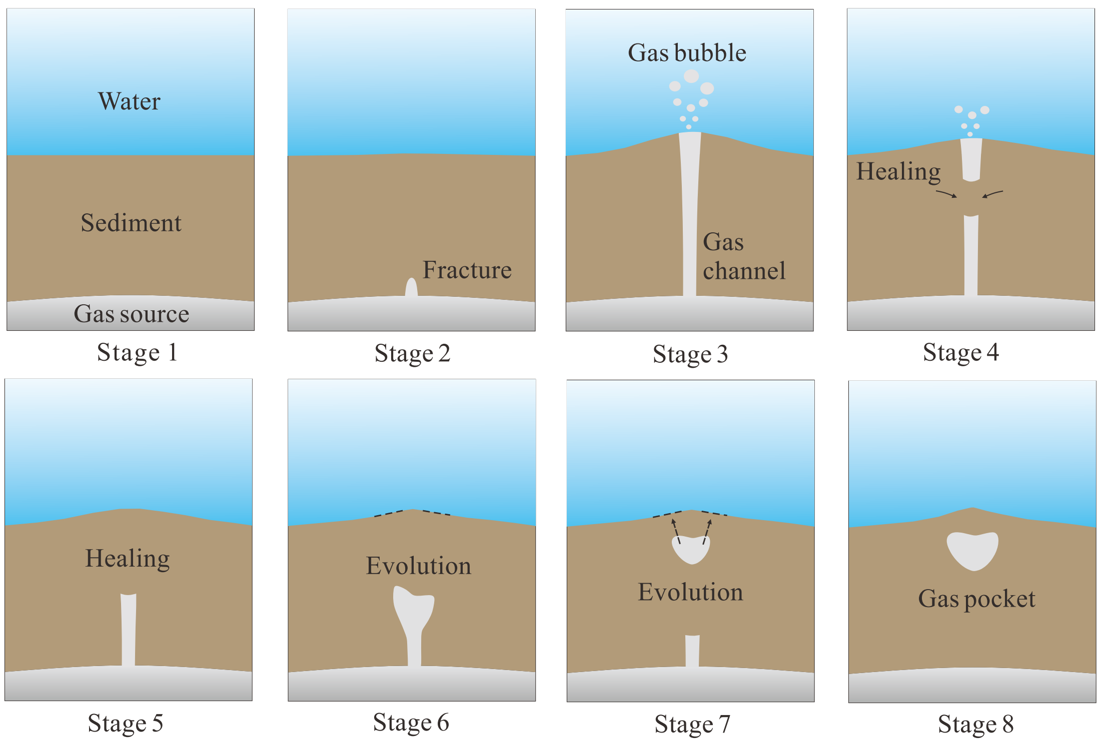

Fig. 13. Conceptual evolution model of submarine knoll formation caused by gas migration (Stages 1 to 8).

of particle volume V_S, bubble size d_B, bubble volume V_B, and a frequency f_d, given as:

$$\frac{F_r(t)}{k\eta L} \sim \sqrt[3]{\frac{V_B}{V_S}} d_B f_d \tag{4}$$

The particle volume V_S is significantly smaller than the gas bubble V_B, resulting in the $F_r(t)$ predominating over buoyancy, as shown in Fig. 12. This dominance of $F_r(t)$ generates a stochastic momentum that drives the particles toward the gas pocket. In fine-grained sediments, this process leads to a gradual filling of the gas pocket by particles, which macroscopically manifests as the “healing” of previously formed channels. Additionally, large gas bubbles tend to accumulate at some distance above the gas injection point rather than remaining near it. This behavior may suggest a preferential migration of larger bubbles away from the immediate vicinity of the injection zone, likely influenced by the sediment’s structural characteristics and the balance of forces acting on the bubble-sediment system.

4.3 Gas morphology evolution model

Our experiments have revealed distinct behaviors of submarine gas migration in sandy sediments corresponding to grain size. In coarse-grained sandy sediments, gas is rapidly released into the water column through capillary action without causing significant changes to the seabed’s geological structure. In contrast, fine-grained sandy sediments, under varying gas flow rates, can give rise to distinct marine landforms, such as pockmarks and submarine knolls. In this section, we focus on submarine knoll as a case study to propose a conceptual model for gas migration and its full evolutionary process in fine-grained sandy sediments, as depicted in Fig. 13.

Gas originating from various sources accumulates in reservoirs beneath the sediments, with rising gas pressure forming an overpressure zone. Once a critical pressure threshold is exceeded, the gas breaches the sediment layer, initiating infiltration. This process triggers shear or tensile failure, resulting in the formation of fractures that act as initial pathways for gas migration. When the gas flow rate exceeds the natural sedimentation rate, sediment particles are scoured away and transported into the water column due to the "Entrainment Effect". This particle removal causes progressive enlargement of the fractures, which eventually develop into continuous transport pathways extending to the seabed surface.

Following the cessation of gas intrusion, the sediment pathway gradually "heals", with particles filling the voids left behind. In the subsequent period, the residual gas channel evolves in a typical manner, progressing toward the concave surfaces of the sediment along the weaker areas of the sedimentary structure. Eventually, a gas pocket is formed that is related to the shape and surface of the sediment.

Furthermore, when secondary gas invasion occurs, the gas migration path often retraces the original route but releases larger amounts of gas into the marine environment, further shaping the seabed morphology. In cases of multiple gas invasion events, the repeated fracturing and healing cycles may lead to the development of more complicated migration networks, thereby significantly enhancing sediment permeability and promoting larger-scale gas venting. The long-term effects of such processes require further validation through numerical modeling or other experiments.

5. Conclusions

This study has investigated the behavior of gas migration and the associated formation of geological features in sandy sediments, utilizing a custom-developed seepage apparatus integrated with CT scanning technology. The imaging provided by this system offers insights into the underlying mechanisms that govern these processes. The main conclusions are as follows:

1) Gas migration behavior in sandy sediments is strongly influenced by sediment particle size and gas flow rate. Finer sediments subjected to higher gas flow rates exhibit particle displacement-dominated migration, where gas flow actively disrupts the sediment fabric. Conversely, coarser sediments or lower flow rates favor pore invasion mechanisms. Notably, surface responses progress systematically with increasing flow rates: From negligible changes, through localized uplift forming knoll-like features, to the development of prominent pockmarks with subsurface elongated channels.
2) Two key mechanisms were revealed-the entrainment effect and channel healing-which informed the development of an evolution model. This model demonstrates that the resulting geological phenomena depend on the interplay between gas flow rate and the natural settling rate of sediment particles, with pronounced healing effects occurring preferentially in fine-grained sediments due to their greater V_B/V_S ratio.
3) Our results establish a direct correlation between subsurface gas pocket morphology and post-migration surface features. Imaging analysis has revealed that gas preferentially migrates along the normal direction toward concave sediment surfaces, exploiting structurally weaker zones. Notably, larger gas pockets consistently accumulate in upper sediment layers rather than near the intrusion point, demonstrating a clear upward migration preference. This behavior likely results from combined buoyancy effects and the formation of preferential gas channels through the sediment matrix.

This work contributes to the understanding of how gas migration influences seabed deformation in sandy sediments; the findings highlight the importance of sediment properties and gas flow dynamics in determining the nature of gas migration and the associated morphological changes in the sediment. It is important to note that the pore-scale conditions in our test cannot fully replicate field-scale due to the low stress level. Nevertheless, the identified mechanism still offers valuable insights into the understanding of special submarine geology phenomena such as pockmark formation or gas chimney development.

In future work, combining physical modeling with advanced techniques, such as centrifuge testing (e.g. Hu et al., 2015), may offer more realistic perspectives on the dynamics of gas migration in complex marine environments.

Acknowledgements

The authors would like to express their sincere gratitude for the financial supported provided by the National Natural Science Foundation of China (No. 52127815), the Natural Science Foundation of Zhejiang Province (No. LR23E090001) and the National Natural Science Foundation of China (No. 51988101).

Additional information: Author's email

binzhu@zju.edu.cn (B. Zhu).

Conflict of interest

The authors declare no competing interest.

References

Algar, C. K., Boudreau, B. P., Barry, M. A. Initial rise of bubbles in cohesive sediments by a process of viscoelastic fracture. Journal of Geophysical Research: Solid Earth, 2011, 116: B04207.

Barry, M. A., Boudreau, B. P., Johnson, B. D., et al. First-order description of the mechanical fracture behavior of fine-grained surficial marine sediments during gas bubble growth. Journal of Geophysical Research: Earth Surface, 2010, 115: F04029.

Biscay, F., Ghoufi, A., Lachet, V., et al. Monte Carlo calcu-

lation of the methane-water interfacial tension at high pressures. The Journal of Chemical Physics, 2009, 131: 124707.
Cai, J., Xia, Y., Lu, C., et al. Creeping microstructure and fractal permeability model of natural gas hydrate reservoir. Marine and Petroleum Geology, 2020, 115: 104282.
Campbell, J. M., Ozturk, D., Sandnes, B. Gas-driven fracturing of saturated granular media. Physical Review Applied, 2017, 8(6): 064029.
Cao, S., Li, X., Jung, J., Li, X. Experimental techniques for studying interfacial dynamics and sediment response during CH_4-CO_2 hydrate replacement. Capillarity, 2025, 15(3): 53-57.
Cartwright, J., Santamarina, C. Seismic characteristics of fluid escape pipes in sedimentary basins: Implications for pipe genesis. Marine and Petroleum Geology, 2015, 65: 126-140.
Choi, J. H., Seol, Y., Boswell, R., et al. X-ray computed-tomography imaging of gas migration in water-saturated sediments: From capillary invasion to conduit opening. Geophysical Research Letters, 2011, 38: L17310.
Clarke, R. H., Cleverly, R. W. Petroleum seepage and post-accumulation migration. Geological Society, London, Special Publications, 1991, 59: 265-271.
Claypool, G, E., Kaplan, I. R. The origin and distribution of methane in marine sediments, in Natural Gases in Marine Sediments, edited by I. R. Kaplan, Springer, Boston, pp. 99-139, 1974.
Claypool, G. E., Kvenvolden, K. A. Methane and other hydrocarbon gases in marine sediment. Annual Review of Earth and Planetary Sciences, 1983, 11: 299-327.
Flohr, A., Schaap, A., Achterberg, E. P., et al. Towards improved monitoring of offshore carbon storage: a real-world field experiment detecting a controlled sub-seafloor CO_2 release. International Journal of Greenhouse Gas Control, 2021, 106: 103237.
Gong, X., Wang, L. Marine Geotechnical Engineering. Beijing, China Architecture and Building Press, 2022. (in Chinese)
Guo, Z., Gao, X., Wu, H., et al. Failure patterns in layered gas-storage systems. Advances in Geo-Energy Research, 2024, 12(3): 183-193.
Holtzman, R., Szulczewski, M. L., Juanes, R. Capillary fracturing in granular media. Physical Review Letters, 2012, 108(26): 264504.
Hu, L., Meegoda, J. N., Li, H., et al. Study of flow transitions during air sparging using the geotechnical centrifuge. Journal of Environmental Engineering, 2015, 141(1): 04014048.
Iglauer, S., Paluszny, A., Pentland, C. H., et al. Residual CO_2 imaged with X-ray micro-tomography. Geophysical Research Letters, 2011, 38: L21403.
Jain, A. K., Juanes, R. Preferential mode of gas invasion in sediments: Grain-scale mechanistic model of coupled multiphase fluid flow and sediment mechanics. Journal of Geophysical Research: Solid Earth, 2009, 114: 08101.
Johnson, B. D., Boudreau, B. P., Gardiner, B. S., et al. Mechanical response of sediments to bubble growth. Marine Geology, 2002, 187(3-4): 347-363.
Kong, D., Fonseca, J. Quantification of the morphology of shelly carbonate sands using 3D images. Géotechnique, 2018, 68(3): 249-261.
Kou, B., Cao, Y., Li, J., et al. Granular materials flow like complex fluids. Nature, 2017, 551(7680): 360-363.
Lei, L., Seol, Y., Choi, J. H., et al. Pore habit of methane hydrate and its evolution in sediment matrix-Laboratory visualization with phase-contrast micro-CT. Marine and Petroleum Geology, 2019, 104: 451-467.
Lenormand, R., Zarcone, C., Sarr, A. Mechanisms of the displacement of one fluid by another in a network of capillary ducts. Journal of Fluid Mechanics, 1983, 135: 337-353.
Lin, Q., Bijeljic, B., Berg, S., et al. Minimal surfaces in porous media: Pore-scale imaging of multiphase flow in an altered-wettability Bentheimer sandstone. Physical Review E, 2019, 99(6): 063105.
Liu, L., Wilkinson, J., Koca, K., et al. The role of sediment structure in gas bubble storage and release. Journal of Geophysical Research: Biogeosciences, 2016, 121(7): 1992-2005.
Lu, T. Research on the microstructural characteristics and seepage simulation of loess in Xi'an, North of China. Xi'an, Chang'an University, 2024. (in Chinese)
Ma, G., Zhan, L., Lu, H., et al. Structures in shallow marine sediments associated with gas and fluid migration. Journal of Marine Science and Engineering, 2021, 9(4): 396.
Mason, G., Morrow, N. R. Capillary behavior of a perfectly wetting liquid in irregular triangular tubes. Journal of Colloid and Interface Science, 1991, 141(1): 262-274.
Orange, D. L., Teas, P. A., Decker, J., et al. The utilisation of seaseep surveys (a defense/hydrography spin-off) to identify and sample hydrocarbon seeps in offshore Frontier Basins. Paper cp-148-00254 Presented at International Petroleum Technology Conference, Kuala Lumpur, Malaysia, 3-5 December, 2008.
Pape, T., Geprägs, P., Hammerschmidt, S., et al. Hydrocarbon seepage and its sources at mud volcanoes of the Kumano forearc basin, Nankai Trough subduction zone. Geochemistry, Geophysics, Geosystems, 2014, 15(6): 2180-2194.
Patzek, T. W. Verification of a complete pore network simulator of drainage and imbibition. SPE Journal, 2001, 6(2): 144-156.
Pau, M., Hammer, Ø., Chand, S. Constraints on the dynamics of pockmarks in the SW Barents Sea: Evidence from gravity coring and high-resolution, shallow seismic profiles. Marine Geology, 2014, 355: 330-345.
Puzrin, A. M., Tront, J., Schmid, A., et al. Engineered use of microbial gas production to decrease primary consolidation settlement in clayey soils. Géotechnique, 2011, 61(9): 785-794.
Roche, B., Bull, J. M., Marin-Moreno, H., et al. Time-lapse imaging of CO_2 migration within near-surface sediments during a controlled sub-seabed release experiment. International Journal of Greenhouse Gas Control, 2021, 109: 103363.

Rogener, M. K., Bracco, A., Hunter, K. S., et al. Long-term impact of the Deepwater Horizon oil well blowout on methane oxidation dynamics in the northern Gulf of Mexico. Elementa: Science of the Anthropocene, 2018, 6: 73.

Seol, Y., Lei, L., Choi, J. H., et al. Integration of triaxial testing and pore-scale visualization of methane hydrate bearing sediments. Review of Scientific Instruments, 2019, 90(12): 124504.

Sirhan, S. T., Katsman, R., Lazar, M. Methane bubble ascent within fine-grained cohesive aquatic sediments: dynamics and controlling factors. Environmental Science and Technology, 2019, 53(11): 6320-6329.

Srivastava, A., Kikuchi, K., Ishikawa, T. Microbial Brazil nut effect. Soft Matter, 2021, 17(46): 10428-10436.

Sultan, N., De, Gennaro. V., Puech, A. Mechanical behaviour of gas-charged marine plastic sediments. Géotechnique, 2012, 62(9): 751-766.

Sultan, N., Plaza-Faverola, A., Vadakkepuliyambatta, S., et al. Impact of tides and sea-level on deep-sea Arctic methane emissions. Nature Communications, 2020, 11(1): 5087.

Sun, Z., Santamarina, J. C. Grain-displacive gas migration in fine-grained sediments. Journal of Geophysical Research: Solid Earth, 2019, 124(3): 2274-2285.

Wang, P., Wang, L., Kong, D., et al. Experimental evaluation of gas production from hydrate-bearing sediments via combined hydraulic fracturing and depressurization method. Gas Science and Engineering, 2025a, 136: 205566.

Wang, S., Kong, D., Tan, J., et al. Mechanisms driving pathway-opening migration of gas in marine clayey sediments. Engineering Geology, 2025b, 348: 107965.

Wei, J., Li, J., Wu, T., et al. Geologically controlled intermittent gas eruption and its impact on bottom water temperature and chemosynthetic communities–A case study in the "HaiMa" cold seeps, South China Sea. Geological Journal, 2020, 55(9): 6066-6078.

Xu, Y., Wu, H., Shen, J., et al. Risk and impacts on the environment of free-phase biogas in Quaternary deposits along the coastal region of Shanghai. Ocean Engineering, 2017, 137: 129-137.

Yan, X. Study of slope deformation and failure induced by gas movement in shallow seabed. Hangzhou, Zhejiang University, 2020. (in Chinese)

Yan, X., Xie, W., Wei, Z., et al. Experimental model of pockmarks from gas hydrate decomposition by aeration. Proceedings of the Institution of Civil Engineers-Maritime Engineering, 2021, 174(1): 4-10.

Yoneda, J., Oshima, M., Kida, M., et al. Permeability variation and anisotropy of gas hydrate-bearing pressure-core sediments recovered from the Krishna-Godavari Basin, offshore India. Marine and Petroleum Geology, 2019, 108: 524-536.